

Covering convection with a thermal blanket

Jinzi Mac Huang^{1,2†}

¹NYU-ECNU Institute of Physics and Institute of Mathematical Sciences, New York University Shanghai, Shanghai, 200124, China

²Applied Math Lab, Courant Institute, New York University, New York, NY 10012, USA

(Received xx; revised xx; accepted xx)

Adding moving boundaries to thermally convective fluids is known to result in nontrivial and surprising dynamics. In this work, we investigate the coupling between a floating plate and the convective fluid below it. Through numerical experiments, we show the motion of this plate is driven by the flow beneath. However the flow structure is also modified by the presence of this plate as it shields the heat from escaping, leading to the “thermal blanket” effect. By analyzing this two-way coupling between moving boundary and fluid, we are able to capture the dynamical behaviors of this plate through a low-dimensional stochastic model. Geophysically, the thermal blanket effect is believed to drive the continental drift, therefore understanding this mechanism has significance beyond fluid dynamics.

Key words: Authors should not enter keywords on the manuscript, as these must be chosen by the author during the online submission process and will then be added during the typesetting process (see <http://journals.cambridge.org/data/relatedlink/jfm-keywords.pdf> for the full list)

1. Introduction

The interior of Earth has fascinated generations of scientists (Plummer *et al.* 2001). Among them, Leonardo da Vinci (1452-1519) was one of the pioneers who noticed the incessant geological movements of our planet, as he observed the presence of marine fossils in the mountains. We now know the continents of Earth do not stay in place and instead undergo tectonic motions, and thermal convection in Earth’s mantle is believed to be the driving force of these motions (Kious & Tilling 1996).

Thermal convection occurs when uneven temperatures of fluid lead to uneven density and buoyancy, so warm fluid rises while cold fluid sinks. The definition of fluids here can be very broad, as modern geologists confirm that even the mantle flows like fluids at a large time scale. The Prandtl number (Pr) there, defined as the ratio between the mantle’s kinematic viscosity and thermal diffusivity, is estimated to be around 10^{23} (Meyers *et al.* 1987).

The core of Earth is much warmer than its surface, and the destabilizing buoyancy is strong enough to drive mantle convection. As a measure of relative strength between buoyancy and viscous effects, the Rayleigh number (Ra) is around 10^6 in the mantle (Selley *et al.* 2005). In the well-studied case of Rayleigh-Bénard convection, such a high Ra is known to lead to turbulent fluid motions (Ahlers *et al.* 2009). With the mantle

† Email address for correspondence: machuang@nyu.edu

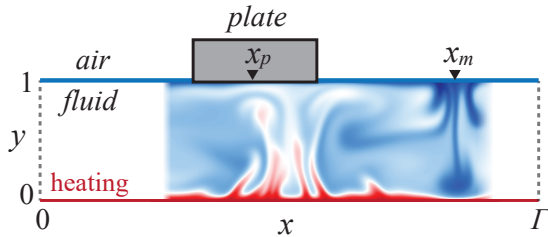


FIGURE 1. Schematics of the moving plate and convecting fluid. The fluid domain is bounded between $y \in (0, 1)$ and periodic in x , and the floating plate of width d has center location x_p .

convecting like a fluid, its surface flow transports the continental plates resulting in their tectonic motions.

Due to the large spatial scale of Earth and the long time scale of mantle convection, the geophysical study of plate tectonics focuses on the current state of continents as well as predicting its important consequences like earthquakes (Plummer *et al.* 2001). On the other hand, numerical simulations (Howard *et al.* 1970; Whitehead 1972; Whitehead & Behn 2015; Mao *et al.* 2019; Mao 2021; Whitehead 2023) and lab-scale experiments (Elder 1967; Zhang & Libchaber 2000; Zhong & Zhang 2005; Whitehead *et al.* 2011) have proven to be an effective means of understanding the dynamics of plate tectonics.

Although the geometry, physical parameters, and time-scales presented in these works are very different from the mantle convection, they reveal surprising dynamics and most importantly, share the same fluid-structure interaction mechanism as the continental drift of Earth. These works confirm that continental plates are not only passive to the mantle flow advection beneath, but are also affecting the flow structure through the *thermal blanket effect*: The continental crust is known to have a much lower heat flux compared to the oceanic crust due to its large crust depth (Mao 2021), so the continental plates essentially serve as a blanket that prevents heat from escaping and warms up the mantle beneath.

How does this thermal blanket effect affect the dynamics of the mantle and continental plates? Why do different continental plates differ in mobility? We address these questions in this article, presenting a numerical investigation along with a simple stochastic model that show how a moving plate mechanically and thermally couples to a convecting fluid flow beneath it.

2. Model and numerical method

2.1. Equations

The configuration of our numerical simulation is shown in Fig. 1, where a solid plate centered at location $x = x_p$ floats on top of a convecting fluid that is bounded in the y direction and periodic in the x direction. Throughout this study, all lengths are rescaled by the fluid depth H , time is rescaled by the diffusion time H^2/κ (κ is thermal diffusivity), and temperature is rescaled by the temperature difference ΔT between the bottom and top free surface. The x direction of the fluid domain is periodic with period $\Gamma = D/H$ (D is the domain width), so the overall computational domain is $x \in (0, \Gamma)$ and $y \in (0, 1)$ as shown in Fig. 1. With the Boussinesq approximation, the resulting PDEs for flow speed

$\mathbf{u} = (u, v)$, pressure p , and temperature $\theta \in [0, 1]$ are

$$\frac{D\mathbf{u}}{Dt} = -\nabla p + \text{Pr} \nabla^2 \mathbf{u} + \text{Ra} \text{Pr} \theta, \quad (2.1)$$

$$\nabla \cdot \mathbf{u} = 0, \quad (2.2)$$

$$\frac{D\theta}{Dt} = \nabla^2 \theta. \quad (2.3)$$

Here, the Rayleigh number is $\text{Ra} = \alpha g \Delta T H^3 / \nu \kappa$ and the Prandtl number is $\text{Pr} = \nu / \kappa$, where ν, α and g are the kinematic viscosity, the thermal expansion coefficient of the fluid, and the acceleration due to gravity. Simple modifications to the flow solver can be adapted for the geophysical mantle convection, but as we wish to consider a more general case of fluid-structure interactions and to apply our theory to future laboratory experiments, we preserve the inertia of both the fluid and the solid plate in this study.

As for boundary conditions, the flow velocity $\mathbf{u} = (u, v)$ is no-slip at the fluid/solid boundary and shear-free at the air/fluid boundary; The temperature θ is 1 at the bottom and 0 at the air/fluid interface. As the plate is shielding the heat from escaping, we take $\theta_n = 0$ beneath it to enforce an adiabatic condition.

The fluid shear force directly drives the plate motion, so

$$m \dot{u}_p = -\text{Pr} \int_P \frac{\partial u}{\partial y}(x, 1, t) dx. \quad (2.4)$$

Here $u_p = \dot{x}_p$ is the plate velocity, $m = \rho d$ is the dimensionless mass of the plate with linear density ρ and width d , and the integration area $P = \{x \mid x \in (x_p - d/2, x_p + d/2)\}$ is the region under the plate.

2.2. Numerical method

The Navier-Stokes equation in 2D can be written in the vorticity & stream function format,

$$\frac{D\omega}{Dt} = \text{Pr} \nabla^2 \omega + \text{Pr} \text{Ra} \frac{\partial \theta}{\partial x}, \quad (2.5)$$

$$-\nabla^2 \psi = \omega, \quad \mathbf{u} = \nabla_{\perp} \psi, \quad (2.6)$$

$$\frac{D\theta}{Dt} = \nabla^2 \theta, \quad (2.7)$$

where the z -component of vorticity $\omega = \hat{\mathbf{z}} \cdot \nabla \times \mathbf{u}$ and the stream function defined by $\mathbf{u} = \nabla_{\perp} \psi = (\psi_y, -\psi_x)$ are solved for, alleviating the difficulty of solving for pressure p .

At the bottom surface $y = 0$, the fluid is no-slip and has a high temperature, so the boundary conditions are

$$\theta = 1, u = v = 0, \psi = \psi_y = 0 \quad \text{at } y = 0. \quad (2.8)$$

At the top surface $y = 1$, the flow is shear-free and has a low temperature at the fluid/air interface. Under the plate, the flow is no-slip and the temperature is flux-free. The boundary conditions are therefore

$$\theta = 0, u_y = v = 0 \quad \text{for } y = 1 \text{ and } x \notin P, \quad (2.9)$$

$$\theta_y = 0, u = u_p, v = 0 \quad \text{for } y = 1 \text{ and } x \in P. \quad (2.10)$$

In the vorticity & stream function format, these conditions can be enforced as

$$\begin{cases} (1 - \mathbb{1}_P)\theta + \mathbb{1}_P\theta_y = 0 \\ \mathbb{1}_P\psi_y + (1 - \mathbb{1}_P)\psi_{yy} = u_p \\ \psi = 0 \end{cases} \quad \text{at } y = 1. \quad (2.11)$$

Here $\mathbb{1}_P$ is an indicator function that take the value of 1 under the plate and 0 otherwise. In the numerical simulations we soften the edge of this indicator function, making it smoother in order to reduce numerical error.

The time derivatives in Eqs. (2.5) and (2.7) are approximated with the second order Adam-Bashforth Backward Differentiation method (ABBD2). At time step $t_n = n\Delta T$, we denote $\omega_n(x, y) = \omega(x, y, n\Delta T)$, $\psi_n(x, y) = \psi(x, y, n\Delta T)$, and $\theta_n(x, y) = \theta(x, y, n\Delta T)$, and Eqs. (2.5) to (2.7) become

$$\nabla^2\omega_n - \sigma_1\omega_n = f_n, \quad (2.12)$$

$$\nabla^2\theta_n - \sigma_2\theta_n = h_n, \quad (2.13)$$

$$-\nabla^2\psi_n = \omega_n, \quad (2.14)$$

where

$$\sigma_1 = \frac{3}{2\text{Pr}\Delta t}, \quad \sigma_2 = \frac{3}{2\Delta t}, \quad (2.15)$$

$$\begin{aligned} f_n = \text{Pr}^{-1} [2(\mathbf{u} \cdot \nabla\omega)_{n-1} - (\mathbf{u} \cdot \nabla\omega)_{n-2}] \\ - (2\text{Pr}\Delta t)^{-1} (4\omega_{n-1} - \omega_{n-2}) - \text{Ra} \left(\frac{\partial\theta}{\partial x} \right)_n, \end{aligned} \quad (2.16)$$

$$h_n = [2(\mathbf{u} \cdot \nabla\theta)_{n-1} - (\mathbf{u} \cdot \nabla\theta)_{n-2}] - (2\Delta t)^{-1} (4\theta_{n-1} - \theta_{n-2}). \quad (2.17)$$

Equations (2.12) to (2.14), together with the inhomogeneous Robin boundary conditions Eqs. (2.8) and (2.11), are Helmholtz equations that can be solved by standard spectral methods (Peyret 2002). More details of this numerical solver will be included in future publications.

Nonlinear terms like $\mathbf{u} \cdot \nabla\theta$ and $\mathbf{u} \cdot \nabla\omega$ in Eqs. (2.16) and (2.17) are computed pseudo-spectrally with a simple and efficient anti-aliasing filter (Hou & Li 2007). With given initial and boundary data, (2.13) can be solved first to obtain θ_n , which is inserted in f_n so (2.12) can be solved next. Finally, (2.14) is solved with the known ω_n .

After solving for the flow and temperature fields, the plate acceleration can be determined as

$$a_{p,n} = -\frac{\text{Pr}}{m} \int_P \frac{\partial^2\psi_n}{\partial y^2}(x, 1)dx. \quad (2.18)$$

The plate velocity $u_{p,n}$ and plate location $x_{p,n}$ can then be computed through a 2nd order Adam-Bashforth method,

$$x_{p,n} = x_{p,n-1} + \frac{\Delta t}{2}(3u_{p,n-1} - u_{p,n-2}), \quad (2.19)$$

$$u_{p,n} = u_{p,n-1} + \frac{\Delta t}{2}(3a_{p,n-1} - a_{p,n-2}). \quad (2.20)$$

In all simulations, we choose $\text{Ra} = 10^6$, $\text{Pr} = 7.9$, $\Gamma = 4$, and $m = 4d$ (d is the plate width), matching the parameters of water convection in experiments (Zhang & Libchaber 2000; Zhong & Zhang 2005). Typically, there are 256 Fourier modes in the x direction

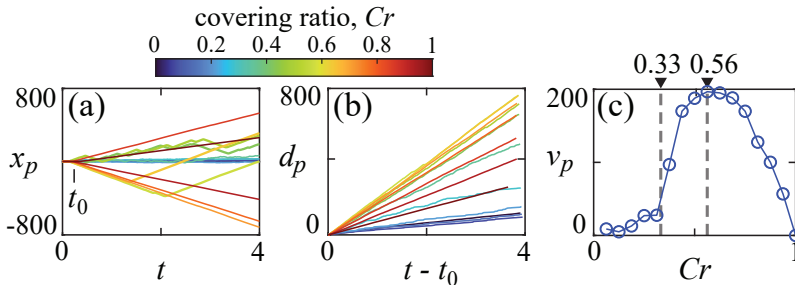


FIGURE 2. Motion of a plate floating on top of a convective fluid. (a) Trajectories of plates of various sizes. The covering ratio is $Cr = d/\Gamma$ and the time t_0 marks the beginning of plate motion. (b) The total displacement of the plates, where d_p is defined through $\dot{d}_p = |\dot{x}_p|$. (c) Average plate speed $v_p = \langle |\dot{x}_p| \rangle$ becomes high when $Cr > 0.33$ and reaches a maximum at $Cr = 0.56$. In these simulations, $\Gamma = 4$, $\rho = 4$, $Ra = 10^6$, and $Pr = 7.9$.

and 64 Chebyshev nodes in the y direction, with a time step size of $\Delta t = 10^{-6}$. These parameters are tested to yield resolved and accurate numerical solutions.

3. Results

3.1. Numerical results

Several trajectories of plates with various sizes are shown in Fig. 2(a), and we can immediately see how the plate's size affects its motion. We define the *covering ratio* $Cr = d/\Gamma$ to measure how much of the free surface is covered by the plate. For small plates, their net displacement is small, which can be better seen from the total displacement $d_p(t) = \int_0^t |u_p(t')| dt'$ shown in Fig. 2(b). Increasing the plate size, linear motion appears as Cr becomes greater than 0.33, as seen in the green trajectories in Fig. 2(a). These trajectories are subject to reversals, as there is an effective noise from the turbulent fluid forcing. As Cr further increases, the linear motion becomes more persistent, as the reversals of plate motion become rare when $Cr \rightarrow 1$ in Fig. 2(a). We note that similar dynamical behaviors have been seen in geophysical Stokes flow simulations (Mao 2021), therefore the coupling mechanism between the moving plate and flow beneath must be similar for different flow regimes.

From the total displacement d_p , one can see that a maximum plate speed is achieved at around $Cr \approx 0.5$, and this can be confirmed by plotting the time-averaged plate speed $v_p = \langle |\dot{x}_p| \rangle$ in Fig. 2(c). The average velocity v_p remains low for small plates, but increases significantly for $Cr > 0.33$ and reaches a maximum around $Cr = 0.5$.

To investigate the transition between dynamical states, the typical flow and temperature distributions in the fluid are shown in Fig. 3. In Fig. 3(a), a small plate with $Cr = 0.125$ is placed on the convecting fluid and it is attracted by the center of downwelling fluid at x_m [Fig. 1], where the surface flow forms a sink. This sink is a stable equilibrium for the plate, as any deviations from this sink will result in a restoring fluid force acting on the plate. The structure of this flow sink can be further seen in Fig. 3(b), where both the y -averaged temperature $\bar{\theta} = \int_0^1 \theta dy$ and the y -averaged vertical flow velocity $\bar{v} = \int_0^1 v dy$ reach their minima.

Following this surface flow pattern, the plate displacement x_p is stochastic as shown in Fig. 3(c). Due to the random forcing from turbulent flows, the plate location is subject to noise that can be seen affecting the plate velocity u_p in Fig. 3(d), whose histogram shows a Gaussian distribution. It is rare but not impossible for the plate to experience a

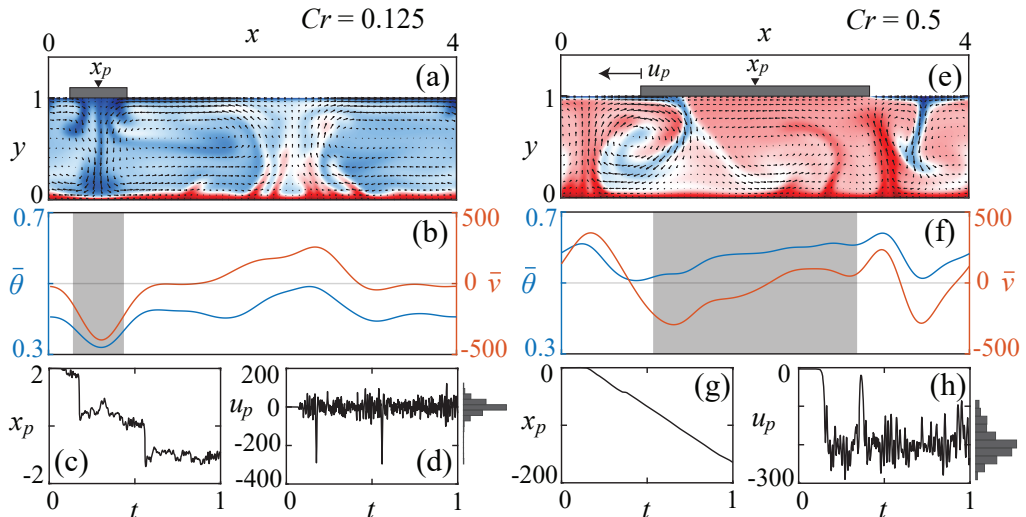


FIGURE 3. Dynamics of floating plate with $Cr = 0.125$ [(a)-(d)] and $Cr = 0.5$ [(e)-(h)]. (a) A typical snapshot of the flow and temperature distributions under the plate with $Cr = 0.125$. (b) The y -averaged temperature and vertical flow velocity corresponding to (a), the shaded area indicates the position of the plate. (c) The plate displacement is a random process. (d) Plate velocity is a random variable with mean 0, whose PDF is a Gaussian distribution as indicated by the histogram. (e) At $Cr = 0.5$, typical flow and temperature distributions showing the plate is transported by the surface flow. (f) The y -averaged temperature and vertical flow velocity corresponding to (e). (g) The plate displacement is linear in time, indicating a unidirectional translation. (h) Plate velocity has nonzero mean. Supplementary movies of these simulations are included.

strong “wind” from the flow, which can push the plate away from the flow sink, across the flow source, and back to the sink again, resulting in the jumps in x_p seen in Fig. 3(c).

Figure 3(e) shows the dynamics of a plate with $Cr = 0.5$. In this case, the plate motion is unidirectional as shown in Fig. 3(g)-(h), with velocity u_p that has a nonzero mean. Shown in Fig. 3(e)-(f), the moving plate tends to situate between the flow sink and source. As the surface flow pushes the plate towards its sink, the distribution of flow temperature also shifts, leading to a moving plate chasing a moving surface flow sink.

This is a direct consequence of the thermal blanket effect: When the plate is large enough, the temperature increases beneath it as heat cannot escape there. This local warming modifies the flow temperature and effectively pushes the cold, downwelling fluid away, resulting in a shift of the flow sink location. Overall, the plate moves towards the cold flow sink while simultaneously pushing the sink away. Thus a simple dynamics exists for this seemingly complicated fluid-structure interaction problem, and we will derive a model from these observations.

3.2. Stochastic model

As seen in Fig. 3, the variation of the y -averaged temperature $\bar{\theta}$ strongly affects the flow pattern. To capture the variational and periodic nature of $\bar{\theta}$, we approximate it with its lowest nontrivial Fourier mode,

$$\bar{\theta}(x, t) = \alpha - \alpha \cos r[x - x_m(t)], \quad (3.1)$$

where x_m is the location of surface flow sink in Fig. 1, $r = 2\pi\Gamma^{-1}$ is the wavenumber, and the constant α measures the strength of temperature variation.

Induced by this temperature distribution, the surface flow velocity $U(x, t) = u(x, 1, t)$

can be approximated as

$$U(x, t) = -\beta \sin r[x - x_m(t)], \quad (3.2)$$

where $\beta > 0$ is the surface flow strength. Indeed, this surface flow profile has a sink at $x = x_m$: Small deviations from x_m results in $U > 0$ for $x < x_m$ and $U < 0$ for $x > x_m$, so the flow locally points towards $x = x_m$.

We note that this surface flow profile does not match the plate velocity at the solid/fluid boundary, and the mismatch between U and u_p allows us to estimate $\partial u / \partial y(x, 1, t)$ and the resulting shear stress, leading to the plate acceleration

$$\dot{u}_p(t) = -\frac{\text{Pr}}{m} \int_P \frac{u_p(t) - U(x, t)}{\delta} dx + \sigma \dot{W}(t). \quad (3.3)$$

Here, δ is the momentum boundary layer thickness (Schlichting & Gersten 2016) that is determined by Ra and Pr , so we assume it to be constant in our study. We also include a white noise with standard deviation σ , representing the turbulent fluid forcing.

To model the moving plate as a thermal blanket, we look at the y -averaged heat equation,

$$\frac{\partial \bar{\theta}}{\partial t} = \frac{\partial^2 \bar{\theta}}{\partial x^2} + q(x, t). \quad (3.4)$$

Here we have ignored the flow advection, and $q(x, t) = \frac{\partial \theta}{\partial y}(x, 1, t) - \frac{\partial \theta}{\partial y}(x, 0, t)$ is the vertical heat flux passing through location x . Assuming the heat leaving the fluid-air interface obeys Newton's law of cooling and no heat penetrates the plate, we can rewrite the heat equation as

$$\frac{\partial \bar{\theta}}{\partial t} = \frac{\partial^2 \bar{\theta}}{\partial x^2} - \gamma \bar{\theta} (1 - \mathbb{1}_P). \quad (3.5)$$

The indicator function $\mathbb{1}_P(x)$ is 1 when $x \in P$ and 0 otherwise, and the constant γ models the rate of cooling. We now plug in the value of $\bar{\theta}$ from Eq. (3.1) and integrate over x , which leads to an ODE for x_m ,

$$\dot{x}_m(t) = \frac{\gamma}{\pi} \int_P [1 - \cos r(x_m - x)] \sin r(x_m - x) dx. \quad (3.6)$$

The integrals in Eqs. (3.3) and (3.6) can be evaluated exactly. Defining a phase angle $\phi = r(x_p - x_m)$, we arrive at a closed dynamical system for (u_p, ϕ) ,

$$\dot{u}_p = -\frac{\beta \lambda}{\pi Cr} \sin(\pi Cr) \sin \phi - \lambda u_p + \sigma \dot{W}, \quad (3.7)$$

$$\dot{\phi} = r u_p + \frac{2\gamma}{\pi} \sin(\pi Cr) \sin \phi - \frac{\gamma}{2\pi} \sin(2\pi Cr) \sin(2\phi), \quad (3.8)$$

where $\lambda = \text{Pr}/(\rho\delta)$. Once the dynamics of (u_p, ϕ) is known, the dynamics of (x_p, x_m) can be calculated through $\dot{x}_p = u_p$ and $x_m = x_p - r^{-1}\phi$.

There are four parameters in this model: β as the strength of surface flow, $\lambda = \text{Pr}/(\rho\delta)$ as a damping coefficient, γ as the rate of surface cooling, and σ as the random fluid forcing. Physically, the surface cooling rate γ is affected by the surface flow strength β , so we take $\gamma = r\beta$ in this model which results in the correct dynamics. The remaining parameters can be estimated from the numerical simulations, and their values and estimation procedures are listed below.

(i) $\beta \approx 400$ is directly measured from the numerical simulation.

(ii) $\lambda \approx 200$ is estimated from $\text{Pr} = 7.9$, $\rho = 4$, and $\delta = 0.01$. The boundary layer thickness δ is estimated from the relation $\delta \sim (2\text{Nu})^{-1}$, where the Nusselt number Nu is at the order of 10^1 as measured from the simulation.

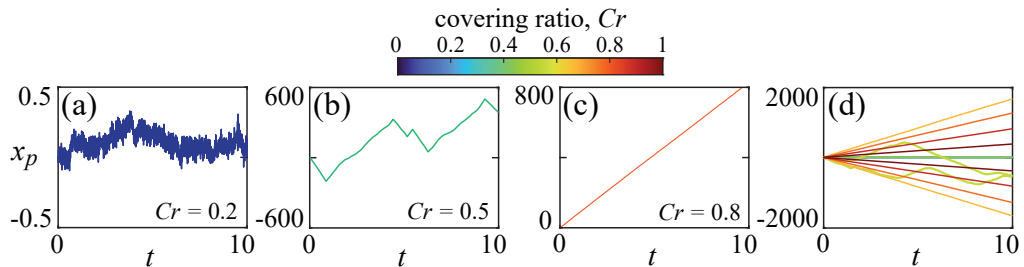


FIGURE 4. Simulated trajectories from the stochastic model. (a) The dynamics of the small plate is a random walk. (b) The medium-sized plate has a nonzero translational velocity whose direction is subject to reversals. (c) The translational motion of the large plate is more persistent. (d) Trajectories of all simulated paths, whose dynamics recover Fig. 2(a).

(iii) $\sigma \approx 200$ is estimated from the variance of the plate center x_p for small Cr . From Eq. (3.7), we have $\sigma^2 \approx 2\lambda\text{Var}(x_p)$, where $\text{Var}(x_p) \approx 100$ is measured from the numerical simulation.

Starting with $\phi(0) = 0$ and a random value of $u_p(0)$, Fig. 4(a)-(c) show some typical trajectories of $x_p(t)$ at different Cr . In Fig. 4(a), the trajectory of the small plate ($Cr = 0.2$) is noise-driven. For the medium plate of $Cr = 0.5$, Fig. 4(b) shows its trajectory is composed of linear translations with reversals. For the large plate of $Cr = 0.8$, Fig. 4(c) indicates that the translation is unidirectional. Furthermore, we plot the typical displacement x_p for plates with various sizes in Fig. 4(d), which resembles Fig. 2(a) and has a transition between the noise-driven and linear motions at $Cr \approx 0.3$. Thus, this simple model captures all the key features of the full numerical simulation.

Without noise, the critical behavior of the dynamical system Eqs. (3.7) and (3.8) can be further analyzed. For small Cr , it is easy to see that Eqs. (3.7) and (3.8) have $u_p = 0$, $\phi = 2\pi N$ (where N is an integer) as equilibria, which are stable and reflect the *passive* state of plate motion. Increasing Cr , new equilibria appear at $Cr^* = 1/3$. For $Cr > Cr^*$, it becomes possible to have a nonzero plate velocity $u_p^* = (\beta/\pi)\hat{u}_p^*$, where

$$\hat{u}_p^* = -\frac{\sin \pi Cr}{Cr} \sin \phi^* \quad (3.9)$$

and the equilibrium ϕ^* can be determined from

$$\cos \phi^* = \frac{1 - (2Cr)^{-1}}{\cos \pi Cr}. \quad (3.10)$$

These states represent the *translation* of the plate. We note that Eqs. (3.9) and (3.10) are only functions of Cr , and thereby independent of all other parameters assumed in this model. To recover the dimensional plate velocity u_p^* , one only needs to know the flow speed factor β/π .

The possible values of \hat{u}_p^* and ϕ^* are shown in Fig. 5. For $Cr < Cr^* = 1/3$, $u_p^* = 0$ and $\phi^* = 2\pi N$ are the only possible equilibria which reflect the passive nature of the small plate that is always attracted by the surface flow sink. For $Cr > Cr^*$, new phases appear as $\phi^* = (2N + 1)\pi \pm \arccos([(2Cr)^{-1} - 1](\cos \pi Cr)^{-1})$, which are solutions of Eq. (3.10) and become stable for large Cr . They indicate that the larger plate tends to sit between the surface flow sink ($\phi = 2N\pi$) and source [$\phi = (2N + 1)\pi$], confirming our observations in Fig. 3. As the surface flow points from its source to its sink [see arrows in Fig. 5(b)], these new phases indicate two possible plate velocities that are given by Eq. (3.9) and shown in Fig. 5(a). Furthermore, Fig. 5(a) resembles Fig. 2(c) as the plate velocity vanishes for $Cr \rightarrow Cr^*$ and $Cr \rightarrow 1$, and obtains its maximum around $Cr = 0.5$.

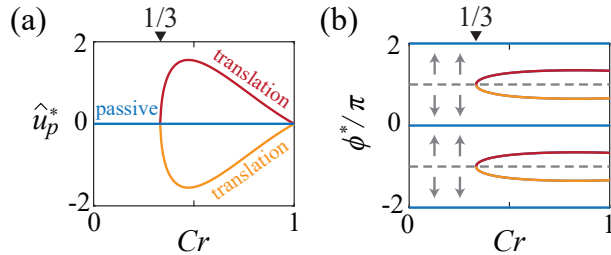


FIGURE 5. Equilibrium values of the plate velocity and phase angle. (a) Dimensionless plate velocity \hat{u}_p is 0 for small Cr , but becomes translational as Cr increases. (b) The phase angle ϕ . Blue lines represent the passive state where the plate is attracted by the flow sink, and red/orange curves show the equilibrium phase of the translational state. The surface flow direction is labelled with arrows.

Through this simple model, we see clear physics of how the solid plate interacts with the fluid beneath: for small plates, the thermal blanket effect is not strong enough and the plate is simply passive to the flow patterns; for large plates, the thermal blanket effect keeps the fluid below it warm while the plate moves towards the surface flow sink, resulting in linear translation.

4. Discussion

In this work, we have numerically explored the mechanical and thermal coupling between a moving plate and a convecting fluid beneath it. Although here we only investigate the dynamics of a single plate, our numerical method is capable of handling multiple plates providing that their interactions can be properly modeled. We are currently investigating such interactions, which has led to even more diverse and unpredictable dynamics. For example, if two small plates each have $Cr < 1/3$ but their combined size reaches $Cr > 1/3$, we have seen that each individual plate moves randomly but their combined “super continent” can translate. In the geophysical case of plate tectonics, plate interactions are the reason for many volcanic activities and mountain formations, therefore understanding the converging and diverging motion of nearby plates might offer new insights into the fluid mechanics behind these geophysical events.

For simplicity, the simulation and model in this work are both two dimensional, and extending our results to three dimensions is a current priority. Using the Chebyshev-Fourier-Fourier method, we have implemented the numerical solver for evolving a plate sitting on top of a three-dimensional domain that is periodic in two horizontal directions. Moreover, the simulation of plate tectonics on a spherical shell is also possible through the Chebyshev-Chebyshev-Fourier method, which is a configuration closer to the geophysical plate tectonics. Through analyzing the direct numerical simulation results there, we wish to further develop our stochastic model and use it to address the fluid-structure interactions happening inside Earth.

Finally, we note that the geophysical plate tectonics is much more complicated than any experiments or numerical simulations conducted so far, as the interior of Earth is such a complex environment and is still being explored by modern science. But although current simple models cannot fully capture the dynamics of continental drifts, they can hopefully still offer some fluid mechanical insights into the geophysics of Earth.

Supplementary Materials

Supplementary movies are available at <https://math.nyu.edu/~jinzi/research/convectivePlate-1p/Movie>.

REFERENCES

- AHLERS, G., GROSSMANN, S. & LOHSE, D. 2009 Heat transfer and large scale dynamics in turbulent Rayleigh-Bénard convection. *Rev. Mod. Phys.* **81** (2), 503.
- ELDER, J. 1967 Convective self-propulsion of continents. *Nature* **214** (5089), 657–660.
- HOU, T. Y. & LI, R. 2007 Computing nearly singular solutions using pseudo-spectral methods. *Journal of Computational Physics* **226** (1), 379–397.
- HOWARD, L., MALKUS, W. & WHITEHEAD, J. 1970 Self-convection of floating heat sources: A model for continental drift. *Geophysical and Astrophysical Fluid Dynamics* **1** (1-2), 123–142.
- KIOUS, W. J. & TILLING, R. I. 1996 *This dynamic Earth: the story of plate tectonics*. DIANE Publishing.
- MAO, Y. 2021 An insulating plate drifting over a thermally convecting fluid: the effect of plate size on plate motion, coupling modes and flow structure. *Journal of Fluid Mechanics* **916**, A18.
- MAO, Y., ZHONG, J.-Q. & ZHANG, J. 2019 The dynamics of an insulating plate over a thermally convecting fluid and its implication for continent movement over convective mantle. *Journal of Fluid Mechanics* **868**, 286–315.
- MEYERS, R. A. *et al.* 1987 *Encyclopedia of physical science and technology*. Academic Press.
- PEYRET, R. 2002 *Spectral methods for incompressible viscous flow*, , vol. 148. Springer Science & Business Media.
- PLUMMER, C. C., MCGEARY, D., CARLSON, D. H. *et al.* 2001 *Physical geology*. McGraw-Hill Boston.
- SCHLICHTING, H. & GERSTEN, K. 2016 *Boundary-layer theory*. springer.
- SELLEY, R. C., COCKS, L. R. M. & PLIMER, I. R. 2005 *Encyclopedia of geology*. Elsevier Academic.
- WHITEHEAD, J., SHEA, E. & BEHN, M. D. 2011 Cellular convection in a chamber with a warm surface raft. *Physics of Fluids* **23** (10), 104103.
- WHITEHEAD, J. A. 1972 Moving heaters as a model of continental drift. *Phys. Earth Planet. In.* **5**, 199–212.
- WHITEHEAD, J. A. 2023 Convection cells with accumulating crust: Models of continent and mantle evolution. *Journal of Geophysical Research: Solid Earth* **128** (4), e2022JB025643.
- WHITEHEAD, J. A. & BEHN, M. D. 2015 The continental drift convection cell. *Geophys. Res. Lett.* **42** (11), 4301–4308.
- ZHANG, J. & LIBCHABER, A. 2000 Periodic boundary motion in thermal turbulence. *Physical Review Letters* **84** (19), 4361.
- ZHONG, J.-Q. & ZHANG, J. 2005 Thermal convection with a freely moving top boundary. *Phys. Fluids* **17** (11), 115105.